



The atmospheric responses to the intensity variability of subtropical front in the wintertime North Pacific

LiYing Wang^{1,2} · HaiBo Hu^{2,3} · XiuQun Yang²

Received: 16 March 2018 / Accepted: 23 September 2018 / Published online: 7 November 2018
© The Author(s) 2018

Abstract

The atmospheric responses to the intensity variability of subtropical front zone (STFZ) in the wintertime North Pacific are investigated in both observation and sensitivity experiments using weather research and forecasting model (version 3.4.1). The STFZ is artificially intensified by applying a sea surface temperature (SST) anomaly within STFZ in sensitivity experiments. Results from observation and experiments indicate that the enhanced STFZ strengthens the meridional temperature gradient and thus the atmospheric baroclinicity, inducing more active transient eddies. The stronger transient eddy vorticity forcing accelerates the polar front jet with equivalent barotropic structure. The results of sensitivity experiments suggest the atmospheric responses are linear and symmetrical to the variation of STFZ intensity within its natural variability. However, the anomalies of atmospheric upstream condition and large-scale SST also have great impacts on the midlatitude atmosphere over North Pacific, in comparison with the effect of STFZ intensity variability. Therefore, It suggests carefully verification of the atmospheric responses found in the observations and numerical experiments.

Keywords North Pacific STFZ · Intensity variation · Synoptic-scale transient eddy · Midlatitude air-sea interaction

1 Introduction

Recent studies have suggested the intimate relationship between the sea surface temperature fronts and the storm tracks in the midlatitude atmosphere (Small et al. 2014; O'Reilly and Czaja 2015; Parfitt et al. 2016). SST fronts can restore the near-surface baroclinicity against the heat flux transport by transient eddies and thus maintain the storm tracks in the midlatitude atmosphere (Nakamura et al. 2008). However, how the atmospheric circulation responds to the variability of SST fronts is still unclear. Frankignoul et al. (2011) suggested that the meridional shift of subarctic

front zone (SAFZ) in the North Pacific generates a barotropic atmospheric response after a two-month lag. Wills et al. (2016) indicated that the SST anomaly (SSTA) near the Gulf Stream front arouses a barotropic atmospheric response over North Atlantic within 2–3 weeks. When the SST in the SAFZ is abnormally warmer in previous autumn, Taguchi et al. (2012) suggest the wintertime storm tracks shift northward as a response, but Gan and Wu (2013) indicated storm tracks in winter appear to be weakened. Small et al. (2014) pointed out that the atmospheric responses to the SST front variability depend on the spatial resolutions of atmospheric model. Therefore, it is still an open question that how and to what extent the atmosphere responds to the variability of SST front.

Many studies evaluated the impacts of SAFZ on the midlatitude atmosphere with a pair of smoothed and unsmoothed SST front experiments (Small et al. 2014; Kuwano-Yoshida and Minobe 2017). Nevertheless, an additional large-scale SST anomaly appears when the SST front is artificially smoothed. It is not clear whether the SST front variability or the large-scale SSTA is responsible for the atmospheric responses. To testify the actual influence of SAFZ variability, Yao et al. (2016) changed the intensity of SAFZ by applying SSTA only around

✉ HaiBo Hu
huhaibo@nju.edu.cn

¹ Zhejiang Meteorological Observatory, Hangzhou 310017, China

² CMA-NJU Joint Laboratory for Climate Prediction Studies, Instituted for Climate and Global Change Research, School of Atmospheric Science, Nanjing University, Nanjing 210093, China

³ Key Laboratory of Meteorological Disaster of Ministry of Education, Nanjing University of Information Science and Technology, Nanjing 210044, China

SAFZ in sensitivity experiments and confirmed the storm tracks can be intensified as a response to the enhanced SAFZ. At present, more attention is paid to the impacts of SAFZ due to its striking intensity (Taguchi et al. 2012; O'Reilly and Czaja 2015), although there is a complicated distribution of SST fronts in wintertime North Pacific: the subtropical front zone (STFZ) around 28°N and SAFZ around 40°N (Nakamura et al. 1997).

Albeit the STFZ is weaker than SAFZ in the wintertime North Pacific, the variability of STFZ can induce a significant atmospheric response (Kobashi et al. 2008; Wang et al. 2016; Zhang et al. 2017). Wang et al. (2016) and Zhang et al. (2017) investigated the relationship between the variability of STFZ intensity and the East Asian jet stream (EAJS) in winter and spring, respectively. Results from observation and sensitivity experiments suggest when STFZ is intensified, the lower-level temperature gradient and atmospheric baroclinicity are enhanced, resulting in more active transient eddy forcing and thus a reinforcement of the EAJS. Wang et al. (2016) also suggested that the low-frequency eddy activities are weakened as a response to the stronger STFZ and attenuate the zonal homogenization of East Asian jet stream (EAJS). Zhang et al. (2017) implied that the intensified convection activities and thus the atmospheric heat source contribute to the acceleration of EAJS. Nevertheless, a large-scale SSTA appears in the sensitivity experiments of both Wang et al. (2016) and Zhang et al. (2017). Therefore, the variability of STFZ intensity may be not the only contributor to the atmospheric responses. In addition, the variation of atmospheric lateral boundary also has influence on the model atmospheric responses (Peng et al. 1997; Msadek et al. 2001). To clarify the actual impact of STFZ intensity variability on the overlying atmosphere, sensitivity experiments without large-scale SST anomalies or atmospheric lateral boundary change are conducted in the present study. Furthermore, the respective effect of the STFZ intensity variability, the large-scale SSTA and the atmospheric lateral boundary change are evaluated with different sensitivity experiments. Section 2 describes the datasets and model used in this study. Section 3 demonstrates the anomalies of surface heat flux and midlatitude atmosphere associated with the variation of STFZ intensity in the observation. The particular introduction of experimental design is present in Sect. 4. Section 5 shows the model atmospheric responses to the intensified STFZ. Section 6 investigates the relative impacts of the STFZ strength variation and atmospheric lateral boundary change. Section 7 presents the conclusion and a briefly discussion about the linearity and symmetry of the atmospheric responses to the STFZ intensity change. Furthermore, a comparison between the atmospheric responses to the anomalies

of STFZ intensity and large-scale SST is also shown in Sect. 7.

2 Datasets and model experiments

Two SST datasets with different spatial resolutions are used to describe the variability of STFZ intensity. One is the Hadley Centre Global Sea Ice and Sea Surface Temperature (HadISST) monthly mean SST data, with relatively coarse spatial resolution of 1.0°. The other is the Optimum Interpolation SST Version 2 (OISST.V2) with relatively fine spatial resolution of 0.25° and temporal resolution of 1 day. Atmospheric anomalies associated with STFZ intensity variability are examined with the 6-hourly European Centre for Medium-Range Weather Forecasts (ECMWF) Interim Reanalysis (ERA-Interim), with a global resolution of 1.5°×1.5°. All datasets are averaged over December, January and February (DJF) to represent wintertime mean during 1982–2010.

The Weather Research and Forecasting Model version 3.4.1 (WRF 3.4.1) is used in this study as the atmospheric regional model. The same model parameterizations are used as in Wang et al. (2016). The model domain is 5°N–60°N, 117°E–117°W, with a relatively high horizontal resolution of 50 km and 28 sigma levels in the vertical. The 6-hourly National Centers for Environmental Prediction (NCEP) Operational Global Final Analyses (FNL) data was prescribed as the model lateral boundaries. The NCEP/FNL reanalysis dataset (<http://rda.ucar.edu/datasets/ds083.2>) was with a spatial resolution of 1.0° × 1.0° and 26 vertical pressure levels from 1000 to 10 hPa.

3 Atmospheric anomalies associated with STFZ intensity variability in observation

3.1 Definition of STFZ intensity index

The climatologies of wintertime SST and its meridional gradient in North Pacific are shown in Fig. 1a, b for HadISST and OISST, respectively. Large values of SST meridional gradient locate along two separated frontal zones, i.e. the STFZ near 28°N and the SAFZ near 40°N. The oceanic fronts from different SST datasets are of similar distribution, except that the gradient in the western SAFZ from OISST is larger than that from HadISST. The SST gradients are zonally-averaged over the North Pacific basin (145°E–145°W) in Fig. 1c. Two extremes exist at about 28°N and 40°N, corresponding to the center locations of the STFZ and SAFZ, respectively. The zonally-averaged SST gradients based on HadISST and OISST datasets are

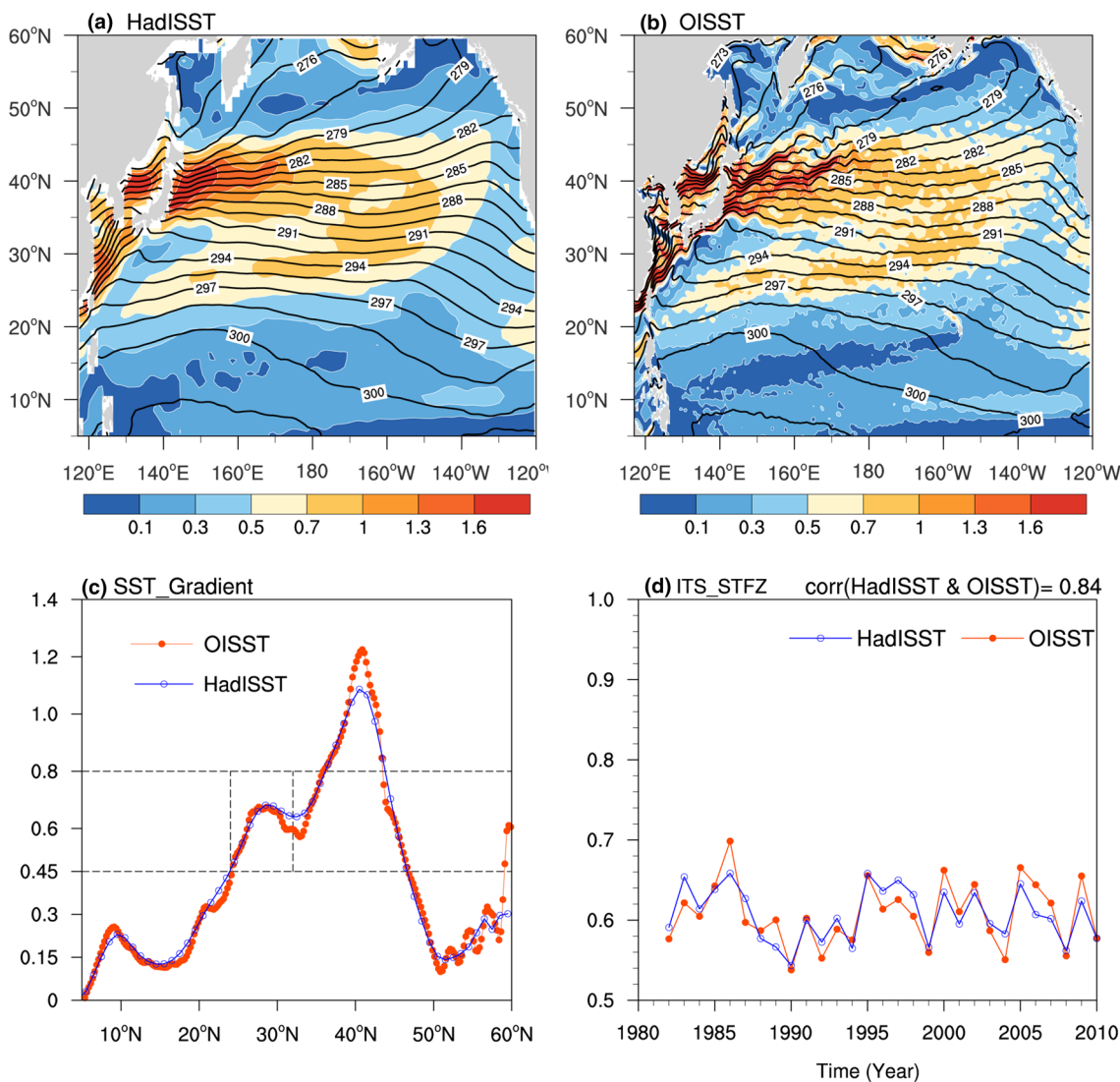


Fig. 1 Climatological distribution of SST (contours, units: K) and its meridional gradient (color shading, units: 10^{-5} km^{-1}) in the wintertime North Pacific, based on **a** HadISST and **b** OISST during 1982–2011. **c** The climatological SST meridional gradient (unit: 10^{-5} km^{-1}) zonally-averaged over 145E–145W as plotted a function of latitude for HadISST (blue line) and OISST (red line). The horizontal line

signifies the empirically-given critical value (0.45) for STFZ intensity index definition, and the vertical lines indicate the latitudinal range (24–32°N) of STFZ for front index definition. **d** Time series of the intensity index of STFZ (units: 10^{-5} km^{-1}) for HadISST (blue line) and OISST (red line) during 1982–2010

basically the same within STFZ (24°–32°N). Follow Wang et al. (2017), the index to quantify the intensity of the STFZ is defined with the zonally-averaged SST gradient within the STFZ. Given STFZ, its intensity for each winter is defined as $\text{ITS} = \sum_{i=1}^N G_i/N$, where G_i is the value of zonally-averaged SST meridional gradient that is no less than an empirically-given critical value (here, $0.45 \times 10^{-5} \text{ K m}^{-1}$ for STFZ) at the i -th latitudinal grid point within the zone, and N is the number of total grid points that satisfy the criteria above. The intensity index reflects an average of the SST meridional gradient within STFZ.

The time series of the intensity index of STFZ (Fig. 1d) characterizes the variability of STFZ strength, where a larger (smaller) index value represents a stronger (weaker) STFZ. The indexes based on two different SST datasets exhibit good consistency during the period 1982–2010.

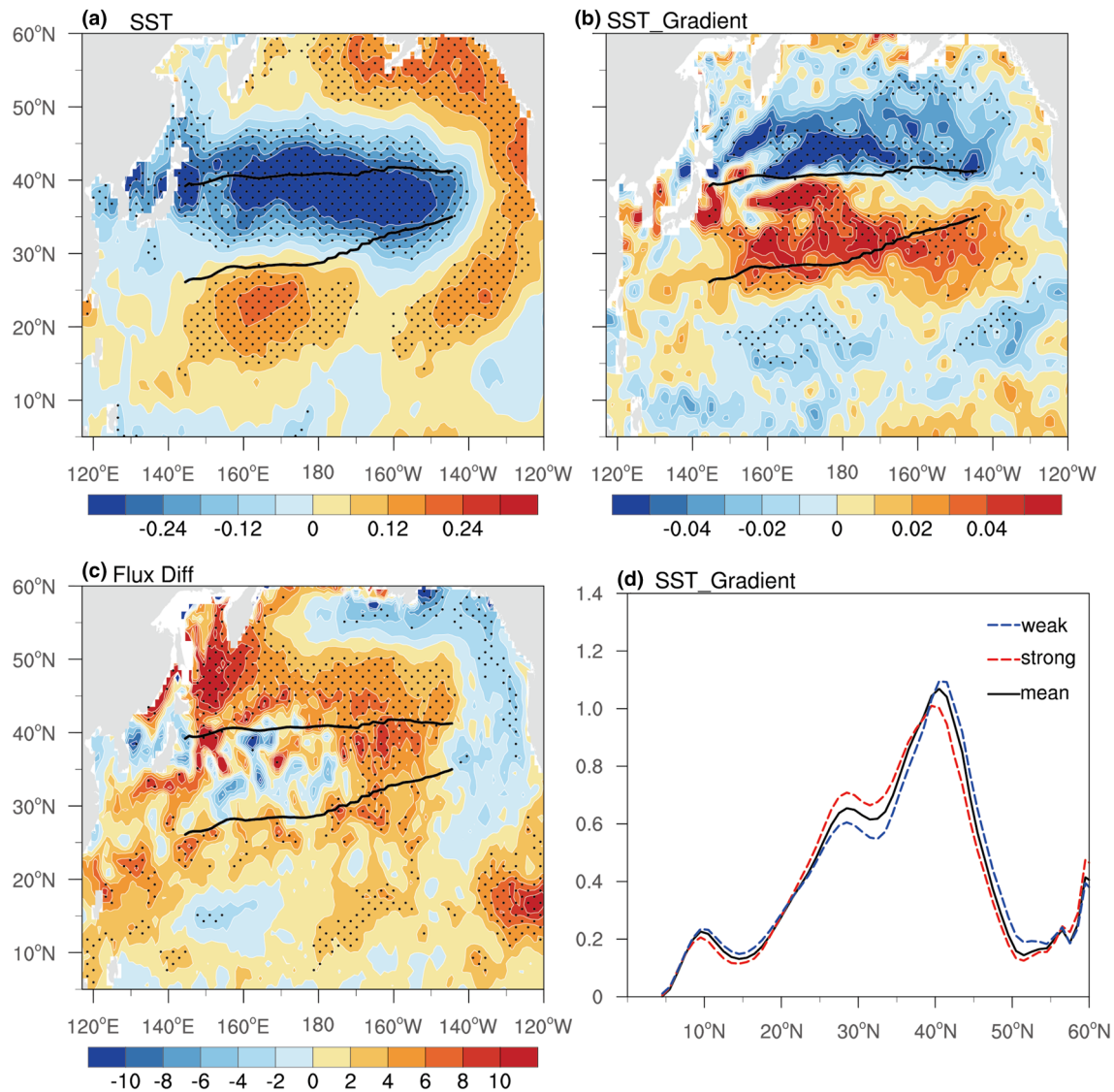


Fig. 2 Spatial distributions of the regressed. **a** SST anomaly (shading, units: K), **b** SST gradient (shading, units: 10^{-5} km^{-1}), **c** total surface flux (shading, Units: W/m^2) upon the intensity index of STFZ. **d** SST gradient zonally-averaged over 145°E – 145°W for strong STFZ year

component (red dotted line), weak STFZ year component (blue dotted line) and climatology (black solid line) during 1982–2010. Areas with statistical significance no less than 90% level are dotted. The climatological locations of STFZ and SAFZ are denoted by black lines

3.2 Relationship between the intensity index of STFZ and the anomalies of SST as well as surface heat flux

The SST anomaly regressed upon the intensity index of STFZ (Fig. 2a) is positive south of 28°N and negative north of 28°N . The dipole distribution of SST anomaly is accompanied with a positive anomaly of SST gradient (Fig. 2b) around STFZ. The negative SST anomaly centers at about 40°N , and the corresponding SST gradient anomaly is of dipole pattern with zero contour around 40°N . When a strong STFZ is present, the SST gradient is intensified south of 40°N and reduced north of 40°N . It tends to induce a southward

shift of SAFZ (Wang et al. 2017). The component of zonally-averaged SST gradient for strong STFZ years (red line in Fig. 2d) presents a weaker and southward shifted SAFZ than climatology (black line in Fig. 2d). The regressed anomaly of surface heat fluxes (sum of sensible and latent heat fluxes, Fig. 2c) is positive (negative) along the south (north) side of STFZ, implying the abnormally warmer (cooler) SST there enhances (weakens) the upward heat flux and forces the overlying atmosphere. At latitude 40° – 50°N , another positive regressed anomaly of surface heat fluxes exists with negative SST anomaly. The stronger upward heat transport from ocean to atmosphere induces heat loss of ocean and leads to the colder SST there. The regression analysis of surface flux

in winter suggests that ocean forces the overlying atmosphere along STFZ, whereas the SST is affected by the atmosphere to the north side of SAFZ.

3.3 Associated atmospheric anomalies with the intensity index of STFZ

Figure 3 shows the atmospheric anomalies regressed upon the intensity index of STFZ, for the meridional air

temperature gradient, atmospheric baroclinicity ($\sigma_{BI} = 0.31 \frac{f}{N} \left| \frac{\partial u}{\partial z} \right|$, Hoskins and Valdes 1990), zonal wind velocity, synoptic-scale eddy kinetic energy ($EKE = (u'^2 + v'^2) / 2$), Kosaka and Nakamura 2008), baroclinic energy conversion ($CP = -\frac{R}{\sigma_0 P} \left(v' T' \frac{\partial \bar{T}}{\partial y} + u' T' \frac{\partial \bar{T}}{\partial x} \right)$, Kosaka and Nakamura 2008), the thermal and vorticity forcings of transient eddy, and the induced tendency of zonal

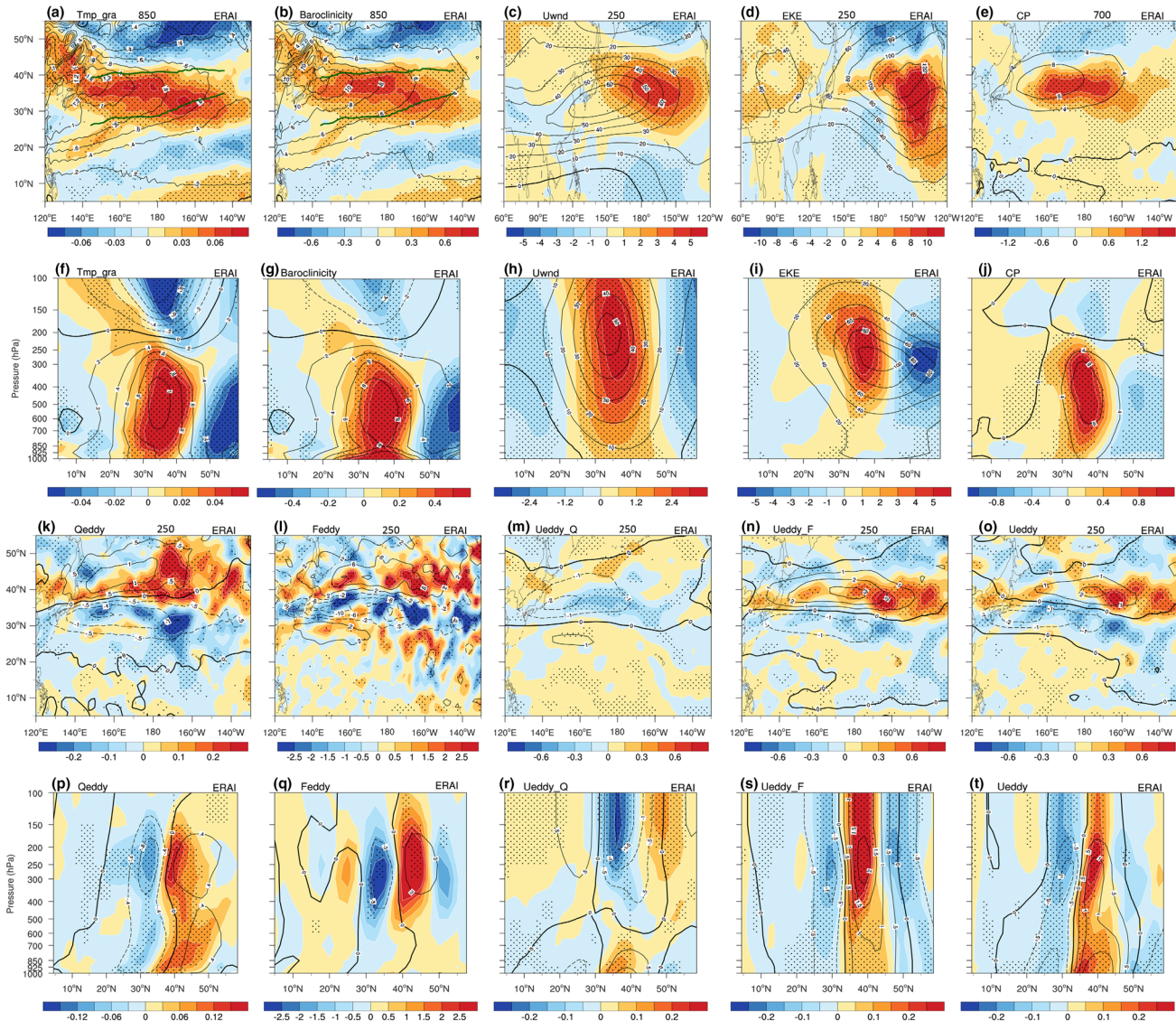


Fig. 3 The horizontal distributions of the climatologies (contours) and the atmospheric anomalies (shading) regressed upon the intensity index of STFZ for **a** air temperature gradient (units: 10^{-5} km^{-1}) at 850 hPa, **b** atmospheric baroclinicity (units: 10^{-5} m^{-1}) at 850 hPa, **c** Zonal wind velocity (units: ms^{-1}) at 250 hPa, **d** EKE (units: $\text{m}^2 \text{s}^{-2}$) at 250 hPa, **e** CP (units: $10^{-4} \text{ m}^2 \text{s}^{-2}$) at 700 hPa, **k** Qddy (units: 10^{-5} K s^{-1}) at 250 hPa, **l** Feddy (units: 10^{-11} s^{-2}) at 250 hPa, **m** $\frac{\partial u}{\partial t}$ induced by eddy vorticity forcing (units: 10^{-5} ms^{-2}) at 250 hPa, **n** $\frac{\partial u}{\partial t}$ induced by eddy total forcing (units: 10^{-5} ms^{-2}) at 250 hPa. The longitudinal range is 60E–120W in **c**, **d**, while is 120E–130W in other panels. The Altitude-latitude distributions of the climatologies (contours) and the atmospheric anomalies (shading) zonally-averaged over 145E–145W regressed upon the intensity index of STFZ are shown in **f–j**, **p–t**, respectively. Areas with statistical significance no less than 90% level are dotted

by eddy vorticity forcing (units: 10^{-5} ms^{-2}) at 250 hPa, **o** $\frac{\partial u}{\partial t}$ induced by eddy total forcing (units: 10^{-5} ms^{-2}) at 250 hPa. The longitudinal range is 60E–120W in **c**, **d**, while is 120E–130W in other panels. The Altitude-latitude distributions of the climatologies (contours) and the atmospheric anomalies (shading) zonally-averaged over 145E–145W regressed upon the intensity index of STFZ are shown in **f–j**, **p–t**, respectively. Areas with statistical significance no less than 90% level are dotted

wind speed, respectively. Here prime denotes the synoptic-scale (2.5–7 day) fluctuations, and overbar denotes the seasonal-mean.

$$\sigma_0 = \frac{1}{C_p} \frac{RT}{p} - \frac{\partial T}{\partial p}$$

gives the hydrostatic stability. The baroclinic energy converts from mean flow to transient eddy when CP is positive, and vice versa. According to the quasi-geostrophic potential vorticity (QGPV) equation (Lau and Holopainen 1984), the tendency of zonal wind velocity can be written as

$$\frac{\partial \bar{u}}{\partial t} = \left[\frac{1}{f} \nabla^2 + f \frac{\partial}{\partial p} \left(\frac{1}{\sigma_1} \frac{\partial}{\partial p} \right) \right]^{-1} \left\{ \frac{1}{\partial y} \left[\frac{\partial}{\partial p} \left(\frac{R}{\sigma_1 p} \bar{Q}_d \right) \right] + \frac{1}{\partial y} \left[\frac{\partial}{\partial p} \left(\frac{R}{\sigma_1 p} \bar{Q}_{eddy} \right) \right] - \frac{1}{f} \frac{\partial \bar{F}_{eddy}}{\partial y} \right\} \quad (1)$$

where \bar{Q}_d is the diabatic heating, \bar{Q}_{eddy} is the transient eddy thermal forcing, $\bar{Q}_{eddy} = -\nabla \cdot (\bar{V}'_h T')$, \bar{F}_{eddy} is the transient eddy vorticity forcing, $\bar{F}_{eddy} = \nabla(\bar{V}'_h \zeta')$. By calculating the 3-D inverted Laplace operator $\left(\left[\frac{1}{f} \nabla^2 + f \frac{\partial}{\partial p} \left(\frac{1}{\sigma_1} \frac{\partial}{\partial p} \right) \right]^{-1} \right)$ with Successive over-relaxation (SOR) method, we get the zonal wind velocity tendency $\left(\frac{\partial \bar{u}}{\partial t} \right)$ induced by each forcing term, respectively.

Climatologically, large values of the meridional temperature gradient (Fig. 3a, f) and atmospheric baroclinicity (Fig. 3b, g) appear in the lower- and mid-troposphere at midlatitudes. The westerly jet prevails over 30°–40°N with equivalent barotropic structure (Fig. 3c, h), which is a combination of the subtropical jet over 32°N and the eddy-driven jet located around 40°N (Fang and Yang 2016). The striking CP in lower- and mid-troposphere over western North Pacific (Fig. 3e, j) suggests baroclinic energy conversion from mean flow to transient eddy and contributes to vigorous transient eddies downstream in higher-troposphere (Fig. 3d, i). The heat flux transport by transient eddies converges north of 40°N while diverges south of 40°N (Fig. 3k, p), acting to weaken the midlatitude temperature gradient. The dipole pattern of transient eddy vorticity forcing with equivalent barotropic structure (Fig. 3l, q) tends to maintain a deep westerly jet around 40°N (Fig. 3n, s). In contrast, the zonal wind speed tendency induced by eddy thermal forcing (Fig. 3m, r) is with a baroclinic structure, which accelerates the westerly jet in lower-troposphere and decelerates the jet in higher-troposphere (Fig. 3n, s). The total effect of transient eddy (Fig. 3o, t) is dominated by eddy vorticity forcing, and tends to produce a zonal wind velocity anomaly with barotropic structure.

Shadings in Fig. 3 present the atmospheric anomalies regressed upon the intensity index of STFZ. The atmospheric anomalies are in phase with their corresponding climatologies, implying their variabilities only in intensity. When STFZ is stronger, the meridional temperature gradient

increases (Fig. 3a, f). The correspondingly stronger atmospheric baroclinicity (Fig. 3b, g) favors for stronger baroclinic energy transformation (Fig. 3e, j) and more vigorous transient eddy activities (Fig. 3d, i), especially downstream of their climatological maximums. As a result, the transient eddy thermal forcing (Fig. 3k, p) and vorticity forcing (Fig. 3l, q) are intensified with barotropic structure, thus moderate the midlatitude temperature gradient and accelerate the zonal wind velocity over 35°–45°N (Fig. 3o, t).

The results from observation are similar with those in

Wang et al. (2016) and Zhang et al. (2017), indicating the intensified STFZ could enhance the low-level baroclinicity and thus the transient eddy activities, resulting in the reinforcement of EAJS. However, as shown in Fig. 2a, the stronger STFZ is accompanied with a large-scale SST anomaly. Besides, the upstream jet (Fig. 3c) and eddies (Fig. 3d) are intensified, when STFZ is stronger. Therefore, the atmospheric anomalies found in observation may not affected only by variability of STFZ intensify. When evaluating the influence of STFZ intensification in numerical experiments, both Wang et al. (2016) and Zhang et al. (2017) simply amplify the strength of STFZ, without considering the potential impacts of other distractions such as large-scale SSTA. In this study, different sensitivity experiments are designed to investigate the actual influence of STFZ intensity variability, and further evaluate the respective effects of STFZ intensity variation, the large-scale SST anomaly, and the atmospheric upstream condition.

4 Experimental design

The NCEP/FNL reanalysis dataset with relatively high spatial resolution is used to reconstruct the SST field in model experiments. The climatology of NCEP/FNL SST field spanning 2000–2010 (Fig. 4a) is of similar distribution with that of OISST and HadISST in Fig. 1a, b. The climatological SST presents a significant zonal-distribution in midlatitude. Based on that, we artificially reconstruct the SST filed by extending the zonally-averaged SST over 145°E–145°W to the whole Pacific basin (Fig. 4b). The distribution of reconstructed SST gradient (blue line in Fig. 4d) is basically consistent with that of observation (black line in Fig. 4d). The reconstructed SST is used to conduct the control experiments (hereafter CNTL). To strengthen the STFZ, SST anomalies (Fig. 4c), positive at the southern side of STFZ (18°N–28°N) with a maximum of 0.5K and the opposite at

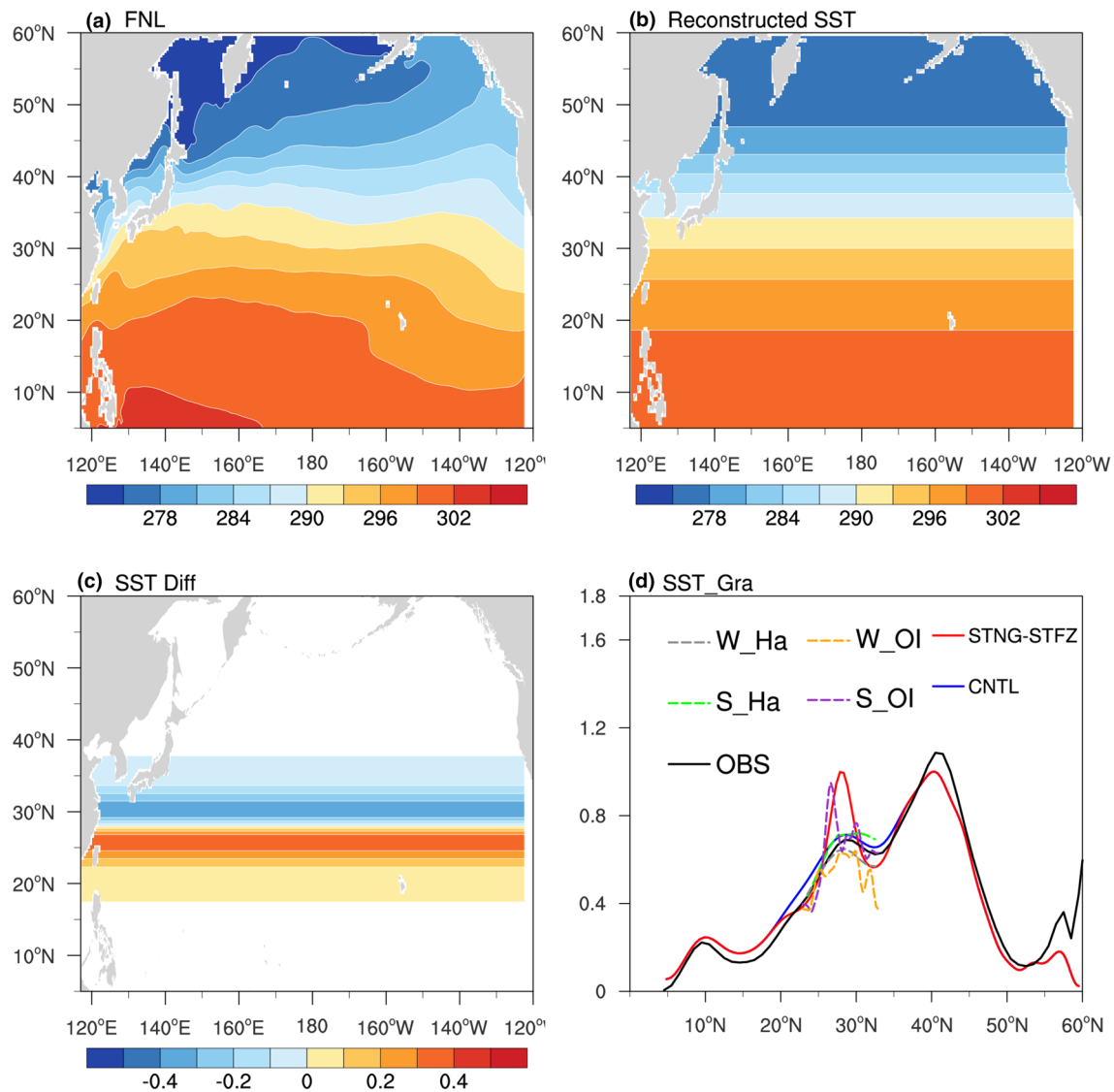


Fig. 4 **a** The climatology of wintertime SST (units: K) based on NCEP/FNL during 2000–2010. **b** The distribution of reconstructed SST (units: K) in CNTL experiment. **c** The SST anomaly (units: K) between STNG-STFZ experiment and CNTL experiment. **d** The meridional gradient of SST zonally-averaged over 145°E–145°W

(units: 10^{-5} km^{-1} , black solid line: observed climatology in HadISST, blue solid line: CNTL, red solid line: STNG-STFZ, green and gray dotted lines denote the strongest and weakest STFZ in HadISST, orange and purple dotted lines denote the strongest and weakest STFZ in OISST)

north (28°N – 38°N), are added to the reconstructed SST. The SSTs in other regions remain unchanged. The SST field with strengthened STFZ (the combination of SST in Fig. 4b and SSTA in Fig. 4c) is used as the SST boundary condition for strengthened STFZ experiments (hereafter STNG-STFZ). When the SSTA is involved, the STFZ is intensified without large-scale SSTA in other region. Therefore, the difference between STNG-STFZ and CNTL experiments can be considered as the actual atmospheric responses to STFZ intensification. The artificially strengthened STFZ (red solid line in Fig. 4d) is comparable to the strongest STFZ appeared in OISST (purple dotted line in Fig. 4d).

Therefore, the STNG-STFZ experiment can be treated as an extreme case of observation. Based on the intensity index on STFZ (Fig. 1d), the year 2002 is picked as a typical strong STFZ year, while the year 1992, 2008 and 2010 are picked as typical weak years. The 6-hourly NCEP/FNL reanalysis data during 01 December 2002 00:00:00 UTC to 28 February 2003 18:00:00 UTC is used as the lateral boundary conditions for both CNTL and STNG-STFZ experiments, to introduce realistic signals of transient eddy activities. We perform a set of 20-ensemble-runs with different initial conditions for each experiment and the ensemble mean is used

Table 1 Introduction to experiment design. A set of 20-ensemble-runs with different initial conditions for each experiment

Experiment classification	Specific experiment design	Experiment name
Control experiments	Reconstructed SST field + atmospheric lateral boundary during 00 UTC 01 December 2002 to 18 UTC 28 February 2003	CTRL
Sensitive experiments	Strengthened STFZ SST field + atmospheric lateral boundary during 00 UTC 01 December 2002 to 18 UTC 28 February 2003	STNG-STFZ

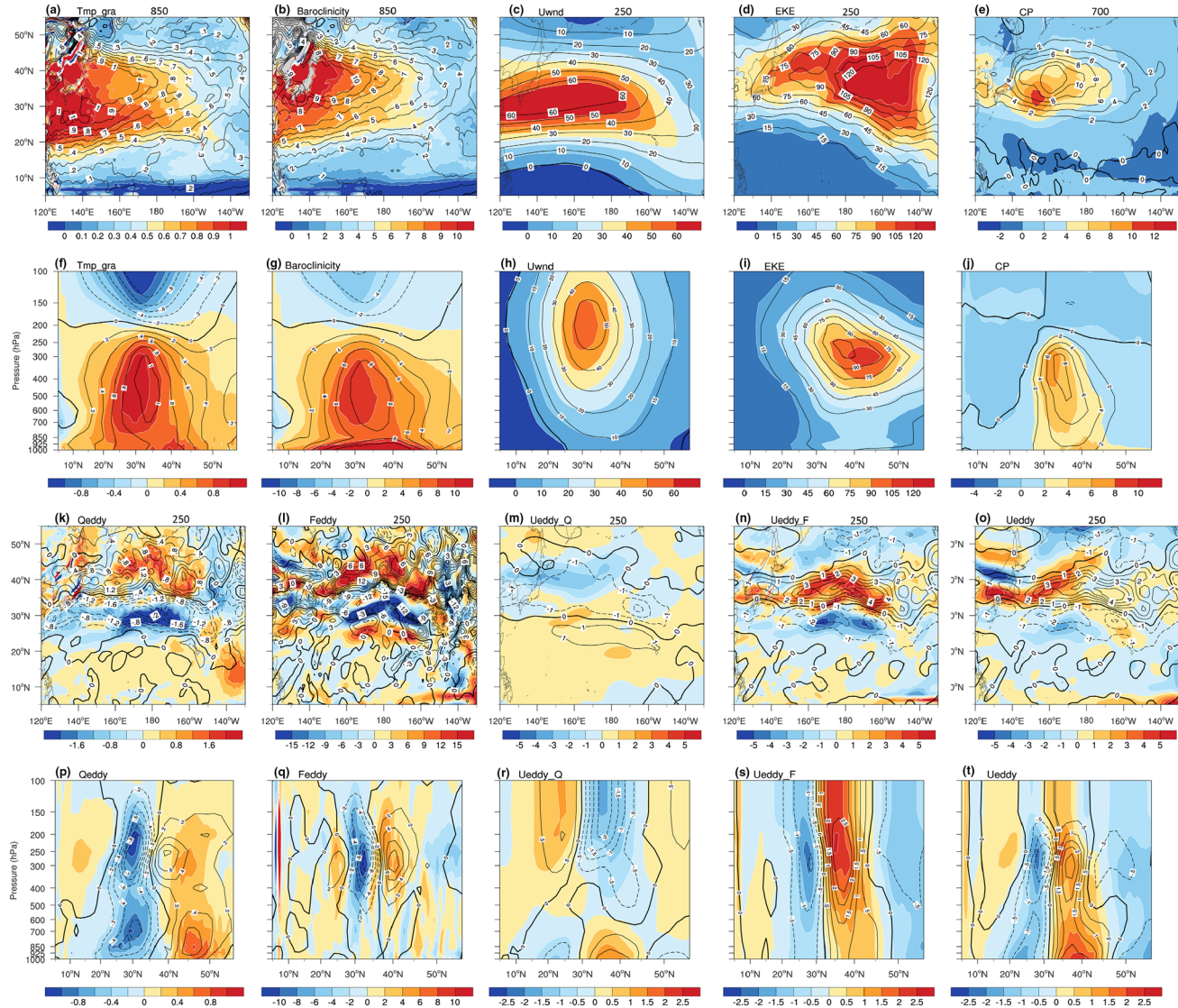


Fig. 5 The horizontal distributions of the observed atmosphere at winter 2002 (contours) and the model atmosphere of CTNL experiment (shading) for **a** air temperature gradient (units: 10^{-5} km^{-1}) at 850 hPa, **b** atmospheric baroclinicity (units: 10^{-5} m^{-1}) at 850 hPa, **c** zonal wind velocity (units: ms^{-1}) at 250 hPa, **d** EKE (units: $\text{m}^2 \text{s}^{-2}$) at 250 hPa, **e** CP (units: $10^{-4} \text{ m}^2 \text{s}^{-2}$) at 700 hPa, **k** Qddy (units: 10^{-5} K s^{-1}) at 250 hPa, **l** Feddy (units: 10^{-11} s^{-2}) at 250 hPa, **m** induced by eddy thermal forcing (units: 10^{-5} ms^{-2}) at 250 hPa, **n** induced by eddy vorticity forcing (units: 10^{-5} ms^{-2}) at 250 hPa, **o** induced by eddy total forcing (units: 10^{-5} ms^{-2}) at 250 hPa. The altitude-latitude distributions of the observed atmosphere at year 2002 (contours) and the model atmosphere of CTNL experiment (shading) zonally-averaged over $145^\circ\text{E} \sim 145^\circ\text{W}$ are shown in **f-j**, **p-t**, respectively

by eddy thermal forcing (units: 10^{-5} ms^{-2}) at 250 hPa, **n** induced by eddy vorticity forcing (units: 10^{-5} ms^{-2}) at 250 hPa, **o** induced by eddy total forcing (units: 10^{-5} ms^{-2}) at 250 hPa. The altitude-latitude distributions of the observed atmosphere at year 2002 (contours) and the model atmosphere of CTNL experiment (shading) zonally-averaged over $145^\circ\text{E} \sim 145^\circ\text{W}$ are shown in **f-j**, **p-t**, respectively

to eliminate the noises. The specific model design for each experiment is demonstrated in Table 1.

The atmospheric distributions in the CNTL experiment (shadings in Fig. 5) are of consistence with observations (contours in Fig. 5), except that the maximum core of air temperature gradient in lower-troposphere locates more southward (along STFZ) in the CNTL experiment (Fig. 5a). It allows us to investigate the atmospheric responses to the variation of STFZ intensity with model simulation in the following section.

5 Atmospheric responses to the strengthened STFZ

Shadings in Fig. 6 show the difference between STNG-STFZ and CNTL experiments, representing the atmospheric responses to the intensification of STFZ. When the STFZ is strengthened, meridional gradient of near-surface temperature is enhanced above the STFZ (Fig. 6f). The positive anomaly of meridional temperature gradient is more obvious

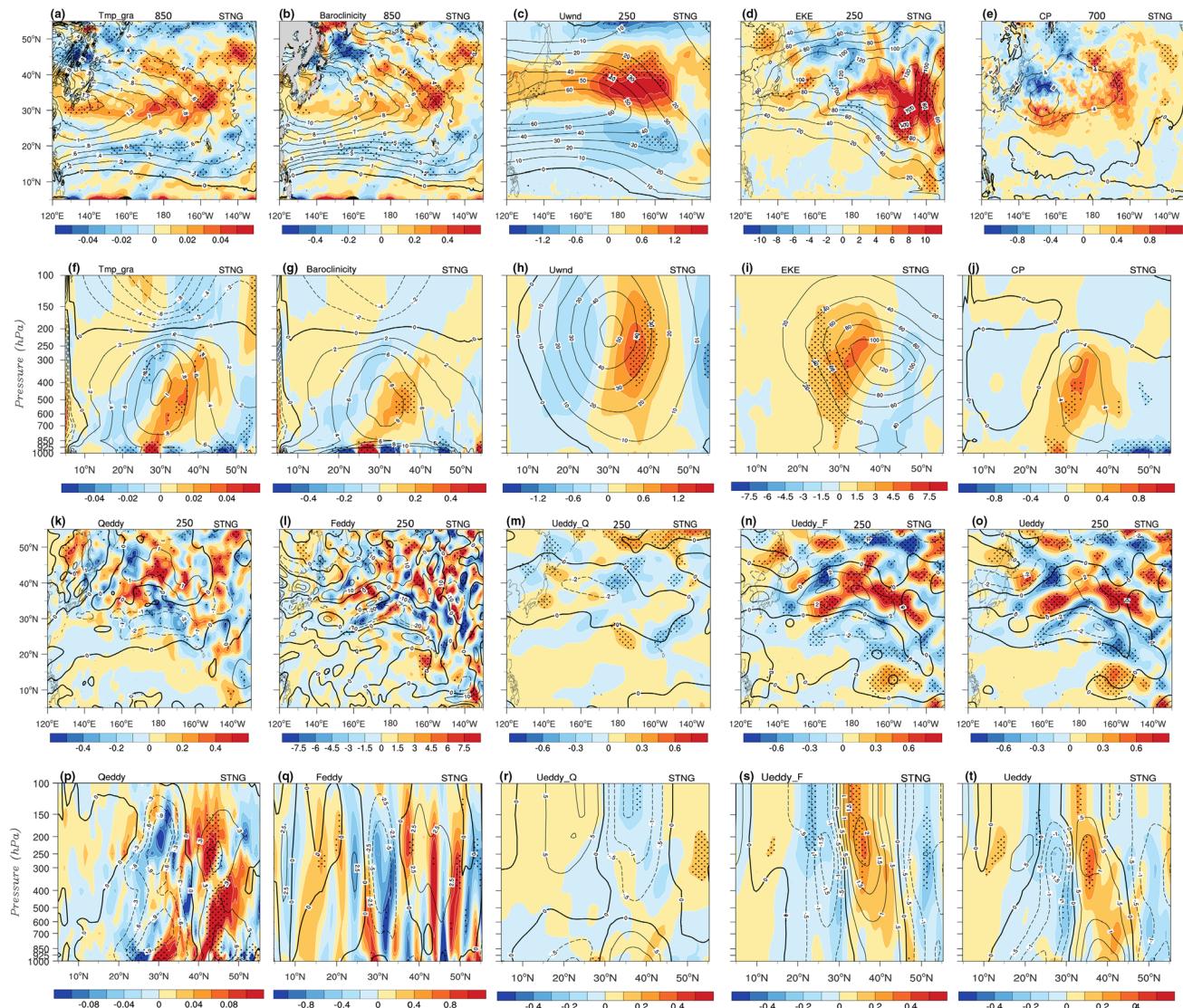


Fig. 6 The horizontal distributions of the atmospheric anomalies (shadings) between the STNG-STFZ and CNTL experiments for **a** air temperature gradient (units: 10^{-5} km^{-1}) at 850 hPa, **b** Atmospheric baroclinicity (units: 10^{-5} m^{-1}) at 850 hPa, **c** zonal wind velocity (units: ms^{-1}) at 250 hPa, **d** EKE (units: $\text{m}^2 \text{s}^{-2}$) at 250 hPa, **e** CP (units: $10^{-4} \text{ m}^2 \text{s}^{-2}$) at 700 hPa, **k** Qeddy (units: 10^{-5} K s^{-1}) at 250 hPa, **l** Feddy (units: 10^{-11} s^{-2}) at 250 hPa, **m** $\frac{\partial u}{\partial t}$ induced by eddy thermal

forcing (units: 10^{-5} ms^{-2}) at 250 hPa, **n** $\frac{\partial u}{\partial t}$ induced by eddy vorticity forcing (units: 10^{-5} ms^{-2}) at 250 hPa, **o** $\frac{\partial u}{\partial t}$ induced by eddy total forcing (units: 10^{-5} ms^{-2}) at 250 hPa. The Altitude-latitude distributions of the atmospheric anomalies zonally-averaged over 145E–145W are shown in **f–j**, **p–t**, respectively. The distributions of wintertime-mean atmosphere in CNTL experiment are shown with contours. Areas with statistical significance no less than 90% level are dotted

Fig. 7 Altitude-latitudinal distributions of the wintertime-mean atmosphere in CNTL experiment (shading) and in SNTV-BDY experiment (contour) at model western boundary (117.5°E) for **a** zonal wind velocity (units: m s^{-1}), and **b** EKE (units: $\text{m}^2 \text{s}^{-2}$)

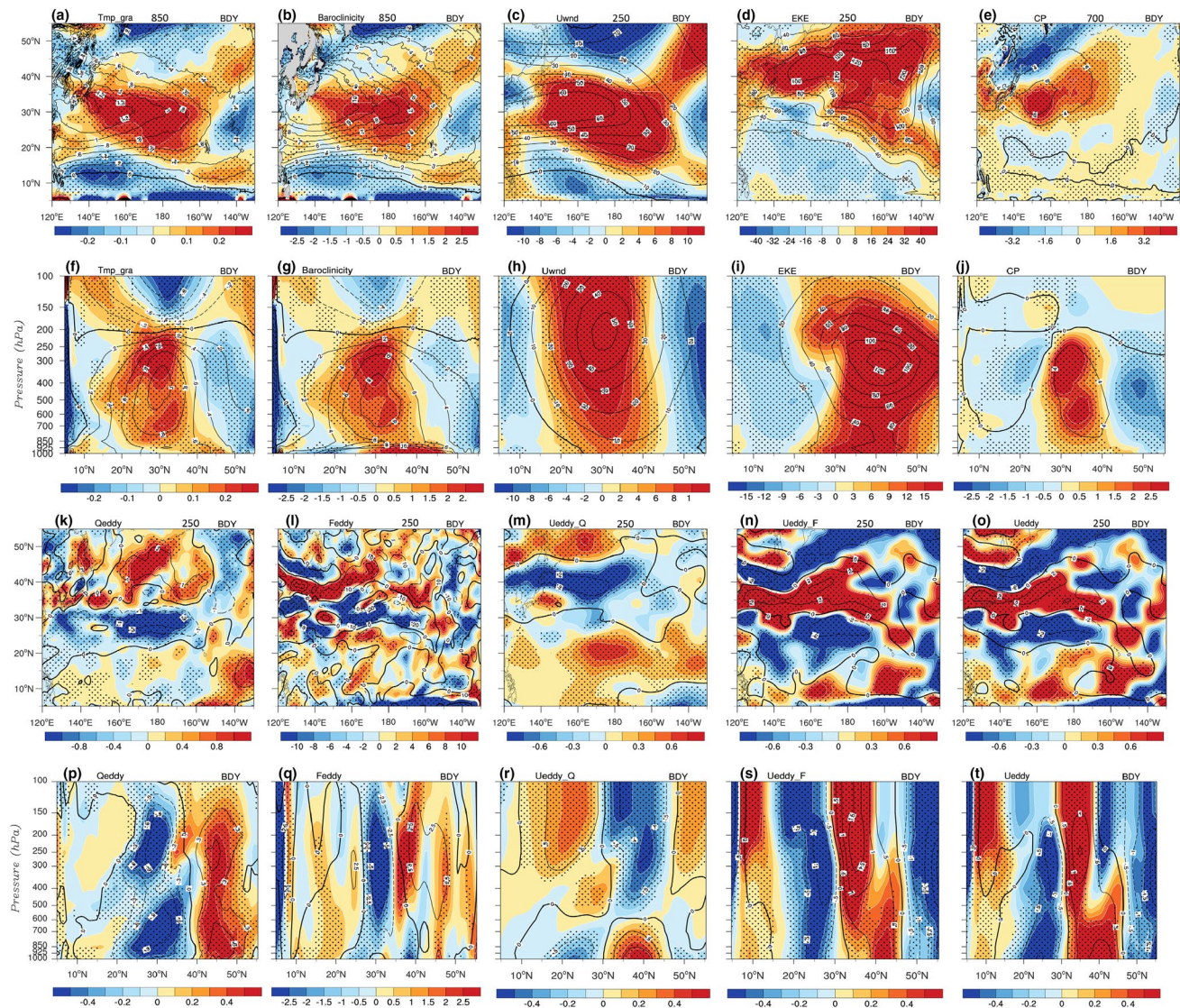
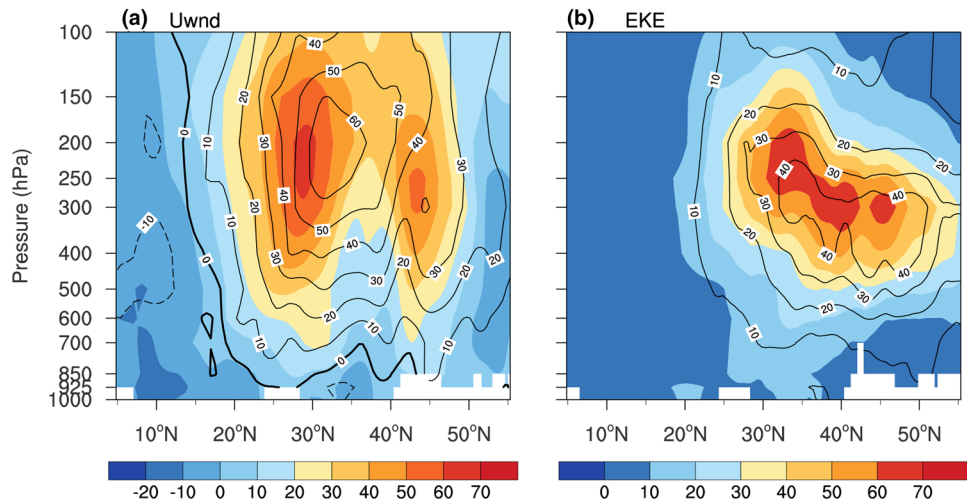


Fig. 8 As in Fig. 6, but for shadings show the atmospheric anomalies between CNTL and SNTV-BDY experiments

in central and eastern North Pacific around STFZ (Fig. 6a), and tilts northward from the lower- to the mid-troposphere (Fig. 6f). The corresponding anomaly of atmospheric baroclinicity (Fig. 6b, g) contributes to stronger baroclinic growth of transient eddies, as implied by the positive anomaly of CP over STFZ in mid- and lower-troposphere (Fig. 6j). The positive response of CP is more evident at central North

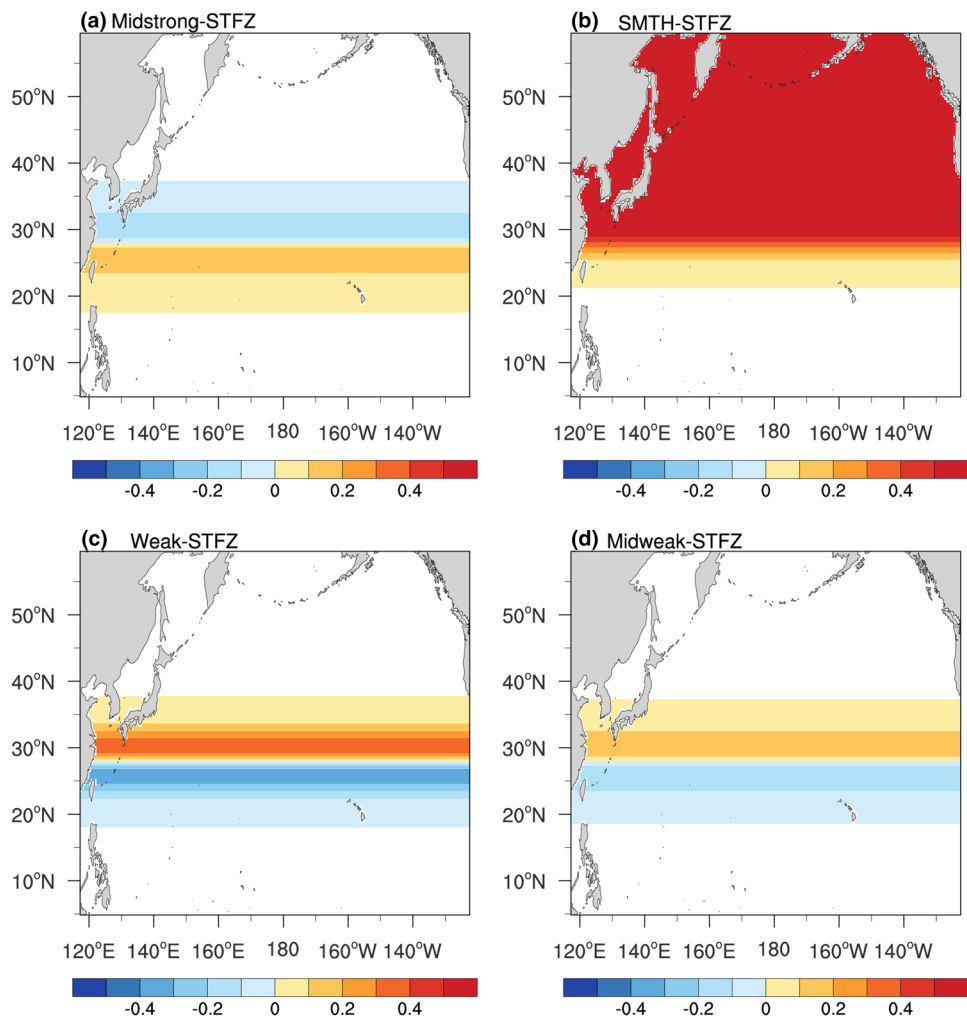
Pacific (Fig. 6e), contributing to more vigorous transient eddy eddies farther downstream (Fig. 6d). The anomalous response of eddy thermal forcing exhibits a meridional dipole pattern near surface with zero contour around STFZ (Fig. 6p) and tilts northwards to its maximum center in mid- and higher-troposphere (Fig. 6k, p). The strengthened eddy thermal forcing tends to moderate the air temperature

Table 2 Introduction to sensitive experiments design

Specific experiment design	Experiment name
Reconstructed SST field + atmospheric lateral boundary during 00 UTC 01 December 1992 to 18 UTC 28 February 1993, 00 UTC 01 December 2008 to 18 UTC 28 February 2009, 00 UTC 01 December 2010 to 18 UTC 28 February 2011, respectively	SNTV-BDY
Mid strengthened STFZ SST field + atmospheric lateral boundary during 00 UTC 01 December 2002 to 18 UTC 28 February 2003	Mid-strong-STFZ
Weakened STFZ SST field + atmospheric lateral boundary during 00 UTC 01 December 2002 to 18 UTC 28 February 2003	Weak-STFZ
Mid weakened STFZ SST field + atmospheric lateral boundary during 00 UTC 01 December 2002 to 18 UTC 28 February 2003	Mid-weak-STFZ
Smoothed SST field + atmospheric lateral boundary during 00 UTC 01 December 2002 to 18 UTC 28 February 2003	SMTH-STFZ

A set of 20-ensemble-runs with different initial conditions for each experiment

Fig. 9 Distributions of SST differences (units: K) between sensitive experiments and CNTL experiment, **a** midstrong-STFZ experiment, **b** SMTH-STFZ experiment, **c** weak-STFZ experiment, **d** Midweak-STFZ experiment



gradient above STFZ and induce a baroclinic zonal wind speed anomaly (Fig. 6m, r). The transient eddy vorticity forcing (Fig. 6l, q) and the induced zonal wind velocity tendency (Fig. 6n, s) get stronger with equivalent barotropic structure over 35° – 45° N. The zonal wind speed tendency induced by total eddy forcing (Fig. 6o, t) is dominated by eddy vorticity forcing, and is of barotropic structure. As a result, a positive anomaly of zonal wind velocity appears north and downstream of jet core (Fig. 6c), with equivalent barotropic structure (Fig. 6h). The distributions of atmospheric responses to the intensified STFZ in numerical experiment are similar with the atmospheric anomalies regressed upon the intensity index of STFZ in observation (Fig. 3). The regression coefficients in Fig. 3 represent the amplitude of atmospheric anomalies when the intensity index of STFZ is enhanced to 1.07 times of climatology in observation. The intensity index of STFZ in STNG-STFZ experiment is reinforced to about 1.09 times of that in CNTL experiment, while the amplitudes of model atmospheric anomalies (Fig. 6) are weaker than that in observation (Fig. 3). The results of STNG-STFZ experiment manifest that the stronger STFZ reinforces the eddy-driven jet via strengthening the low-level baroclinicity and transient eddy vorticity forcing. In the following section, we further investigate the potential reason for the amplitude difference of atmospheric responses between sensitivity experiments and observation.

6 The influence of model lateral boundary condition

When investigating the atmospheric anomalies accompanied with stronger STFZ in observation, significant positive anomalies of jet and eddies appear upstream of North Pacific (Fig. 3c, d), probably inducing atmospheric responses downstream. We wonder whether the anomaly of atmospheric upstream condition contributes to the amplitude difference of atmospheric anomalies between observation and STNG-STFZ experiment. To investigate the potential influence of atmospheric upstream condition, a set of experiments (dubbed as SNTV-BDY experiment) are conducted with the atmospheric lateral boundary of typical weak STFZ years (1992, 2008 and 2010), and the average of simulated results is used. The SNTV-BDY experiments are conducted with the reconstructed SST filed of CNTL experiment. A set of 20-ensemble-runs with different initial conditions is performed for SNTV-BDY experiment. The difference between CNTL and SNTV-BDY experiments indicates the effect of atmospheric lateral boundary variability on the model atmosphere.

Figure 7 demonstrates the contrasts of the zonal wind velocity and EKE at model western boundary from CNTL and SNTV-BDY experiments, respectively. The inflow

westerly jet in SNTV-BDY is stronger, with a maximum about 67 ms^{-1} , and the location of jet core is further northward (Fig. 7a). Figure 7b shows that the introduced transient eddy activities from upstream are more energetic in CNTL experiment than SNTV-BDY experiment.

The differences between CNTL and SNTV-BDY experiments (Fig. 8) imply the atmospheric responses to the variation of atmospheric lateral boundary. The obviously stronger meridional temperature gradient (Fig. 8a, f) and atmospheric baroclinicity (Fig. 8b, g) contribute to energetic transient eddy activities downstream. Together with the stronger eddies introduced from upstream, the EKE is more prominent over the whole basin in CNTL experiment (Fig. 8d, i), leading to an evident acceleration of polar front jet (Fig. 8o, t). Although the jet of CNTL experiment is weaker over 30° – 40° N at the model western boundary, the westerly jet downstream is stronger (Fig. 8c), probably due to the striking transient eddy forcings. The atmospheric responses to the lateral boundary change (Fig. 8) are consistent with observation (Fig. 3), and are stronger in comparison with the atmospheric responses to the variation of STFZ intensity (Fig. 6). The effect of intensified STFZ could be easily covered by the change of atmospheric upstream condition. Therefore, it is not easy to figure out the actual effect of STFZ intensity in the observation.

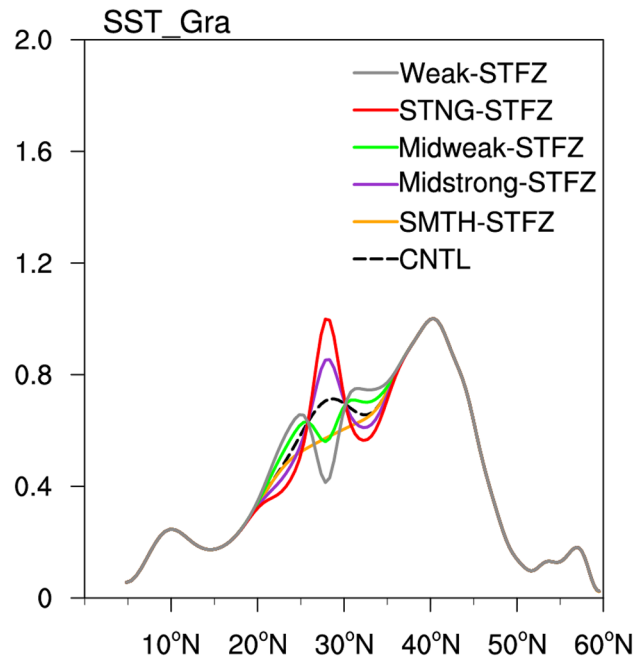


Fig. 10 The meridional gradients of SST zonally-averaged over 145°E – 145°W (units: 10^{-5} km^{-1} , black line: CNTL, orange line: SMTH-STFZ, purple line: midstrong_STFZ, green line: midweak_STFZ, red line: STNG_STFZ, grey line: weak_STFZ)

7 Summary and discussion

Based on the intensity index of STFZ, the atmospheric responses to the variation of STFZ intensity are investigated in both observation and numerical experiments. The intensified STFZ in sensitivity experiments is performed with a dipole pattern of SST anomaly only around STFZ, in order to avoid the distraction of large-scale SST anomaly. When STFZ is intensified, the meridional air temperature gradient and atmospheric baroclinicity are significantly increased, devoting to a stronger transient eddy activity and eddy forcings, thus an acceleration of westerly jet with equivalent barotropic structure. The potential effects of atmospheric upstream condition are further discussed with sensitivity experiments. The atmospheric responses to the anomaly of atmospheric lateral boundary are in phase with but stronger than the atmospheric anomaly to the variation of STFZ intensity. The effect of intensified STFZ could be easily covered by the change of atmospheric upstream

condition. Although the effects of STFZ intensity variability and atmospheric upstream condition are investigated separately from numerical experiments, the potential interaction between these two factors is not discussed in the present study. The upstream eddy variability could arouse an anomaly in STFZ, via altering the surface wind speed and air-sea heat flux around STFZ and hence moderate the SST, and then the anomalous STFZ could give feedback to the overlying atmosphere. We will further investigate the interaction between upstream eddy variability and STFZ variation in the future study.

When investigating the atmospheric responses to intensified STFZ in SNTG-STFZ experiment, we wonder whether the atmospheric responses are linear to different STFZ strength, and whether the atmosphere responds symmetrically to a weakened STFZ? The linearity and symmetry of the atmospheric responses to the variation of STFZ intensity are investigated with sensitivity experiments shown in Table 2. The SST anomaly (Fig. 9a) with half amplitude of the SSTA in STNG-STFZ experiment

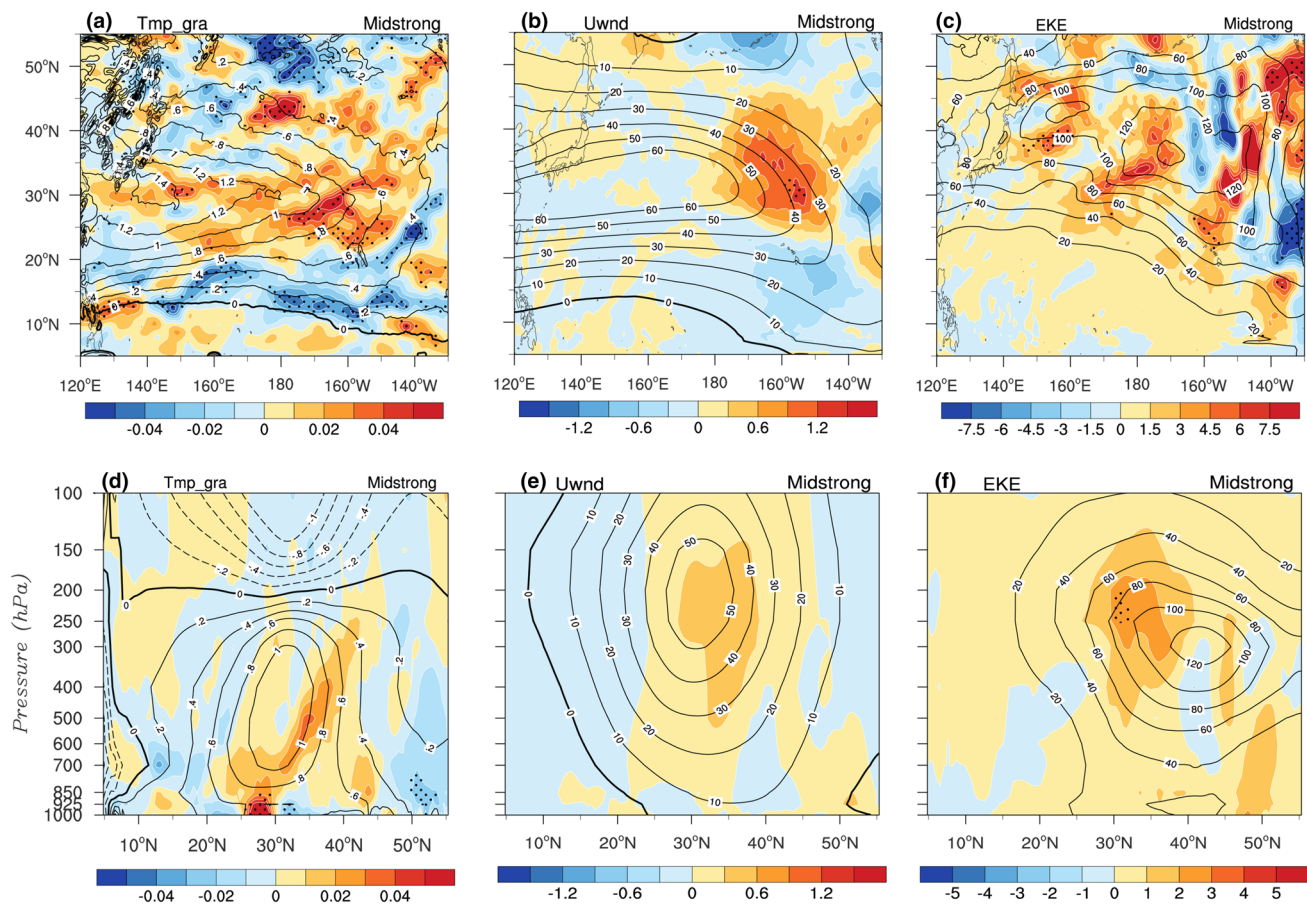


Fig. 11 The horizontal distributions of the atmospheric anomalies (shadings) between the Midstrong-STFZ and CNTL experiments for **(a)** air temperature gradient (units: 10^{-5} km^{-1}) at 850 hPa, **b** zonal wind velocity (units: ms^{-1}) at 250 hPa, **c** EKE (units: $\text{m}^2 \text{s}^{-2}$) at

250 hPa. The Altitude-latitude distributions of the atmospheric anomalies zonally-averaged over 145E–145W are shown in **d–f**, respectively. The distributions of wintertime-mean atmosphere in CNTL experiment are shown with contours

is used in Mid-strong-STFZ experiment (purple line in Fig. 10). The atmospheric responses in Mid-strong-STFZ experiment (Fig. 11) are of the same distribution with STNG-STFZ experiments (Fig. 6) but weaker (about a half) in amplitude, suggesting the midlatitude atmosphere responds linearly to the variability of STFZ intensity.

When an exactly opposite SSTA (Fig. 9c) is involved, the SST gradient is reduced at the center of STFZ but stronger at the north and south sides in Weak-STFZ experiment (gray line in Fig. 10). The anomaly of air temperature gradient is negative south and downstream of its maximum center (Fig. 12a, d), leading to a negative anomaly of EKE downstream (Fig. 12c, f). The westerly jet is reduced with equivalent barotropic structure (Fig. 12b, e). The atmospheric responses of Weak-STFZ are roughly opposite to the results of STNG-STFZ experiment. In Mid-weak-STFZ experiment, the SSTA (Fig. 9d) is half of the SSTA in Weak-STFZ experiment. The atmospheric anomalies of Mid-weak-STFZ experiment (Fig. 13) are of similar distribution and weaker than those in Weak-STFZ experiment. The sensitive experiments imply that the atmospheric responses to the variation of STFZ intensity are linear and symmetrical. Therefore, the

exaggerated intense of STFZ in STNG-STFZ experiment merely amplifies the realistic responses in observation and makes them more visible.

One more set of sensitive experiment is conducted with the smoothed STFZ by meridionally smoothing the SST field and is dubbed as SMTM-STFZ. This method is widely used when investigating the influence of SAFZ in the past studies. When STFZ is smoothed, the SSTA is of large scale and is much stronger than the SSTA in other experiments (Fig. 9b). The difference between CNTL and SMTM-STFZ experiments (Fig. 14) includes the atmospheric responses to the weakened STFZ as well as the large-scale SST anomaly. The amplitudes of atmospheric responses in SMTM-STFZ experiment are stronger in comparison with the result of Weak-STFZ experiment, implying the obvious influence of large-scale SST anomaly beyond the range of STFZ. Therefore, it is more reasonable to inquire the actual effect of SST front by applying SSTA within finite area around oceanic front zone. The atmospheric anomalies associated with STFZ intensity variability in observation are probably the combination of atmospheric responses to the variation

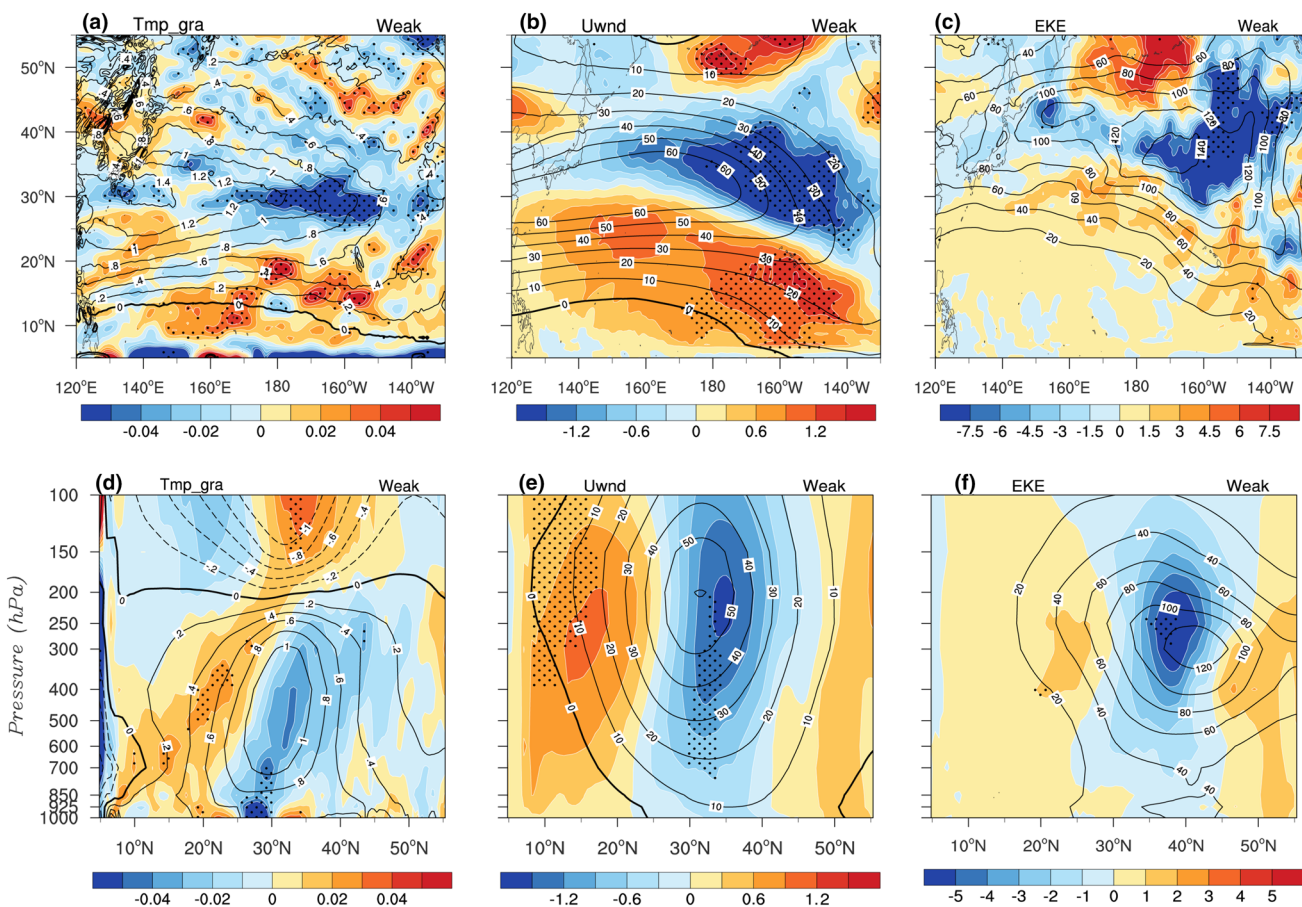


Fig. 12 As in Fig. 10, but for shadings show the atmospheric anomalies between Weak-STFZ and CNTL experiments

of STFZ intensity, the anomalies of atmospheric upstream condition and large-scale SST.

The regression coefficient between the surface heat fluxes and the intensity index of SAFZ implies the ocean forces the overlying atmosphere along SAFZ in the central and eastern North Pacific, but the opposite in western North Pacific. The more significant relationship between surface heat fluxes and the intensity index of STFZ implies that the ocean to atmosphere forcing may be more obvious along STFZ than SAFZ. When the SAFZ is intensified with similar method as for STFZ in simulation, the air temperature gradient and thus atmospheric baroclinicity are intensified along the north side of their maximum core, contributing to the northward shift of the atmospheric front, baroclinic zone, and thus the eddy-driven jet. The simulated results of stronger SAFZ are consistent with the results found in observation (Wang et al. 2017). The intensified SAFZ tends to induce a meridional shift of atmospheric response, whereas the stronger STFZ acts to arouse an atmospheric variability in intensity. Therefore, we think the atmospheric response to the variability of

STFZ intensity in this study is independent of the SAFZ intensity variation.

Yao et al. (2016) intensified the SAFZ in sensitivity experiments and found that the storm tracks are strengthened and northward shifted as response. When the SAFZ strength is reinforce to 1.5 times in Yao et al. (2016), the overlying storm tracks (37° – 42° N) increases about 8%. In this study, the maximum SST gradient of STFZ is enhanced to about 1.4 times (the maximum of STFZ in CNTL experiment is $0.7 \times 10^{-5} \text{ K m}^{-1}$, and in STNG-STFZ is $1.0 \times 10^{-5} \text{ K m}^{-1}$), the storm track response above STFZ increases about 6%. The strength of local storm track response to the strengthened STFZ is comparable with that to the intensified SAFZ in Yao et al. (2016). Therefore, the influence of STFZ intensity anomaly should not be neglected when investigating the impact of North Pacific SST front variability. Further numerical experiments will be conducted to understand the influence of the synergic variability of SST fronts in North Pacific.

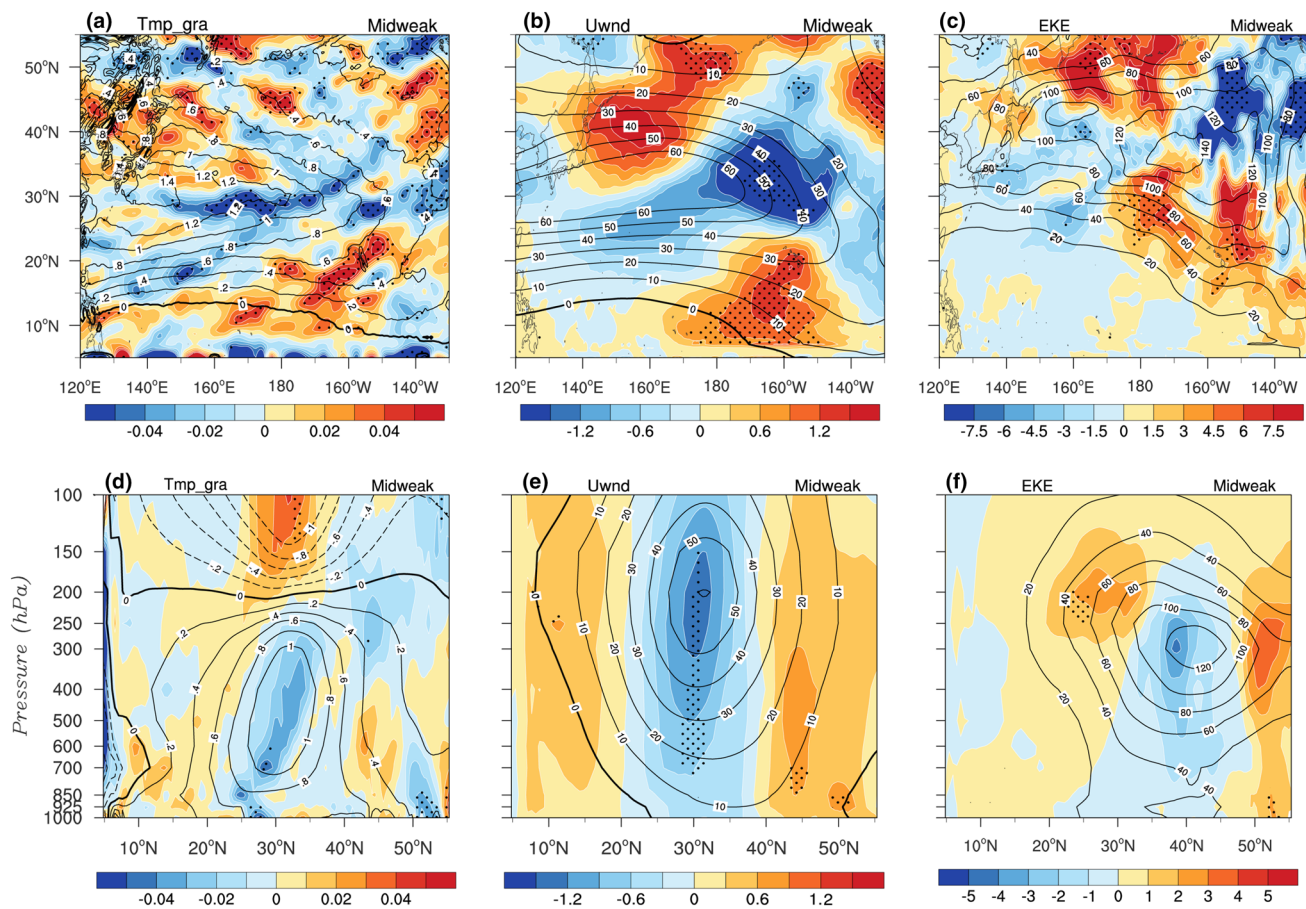


Fig. 13 As in Fig. 10, but for shadings show the atmospheric anomalies between Midweak-STFZ and CNTL experiments

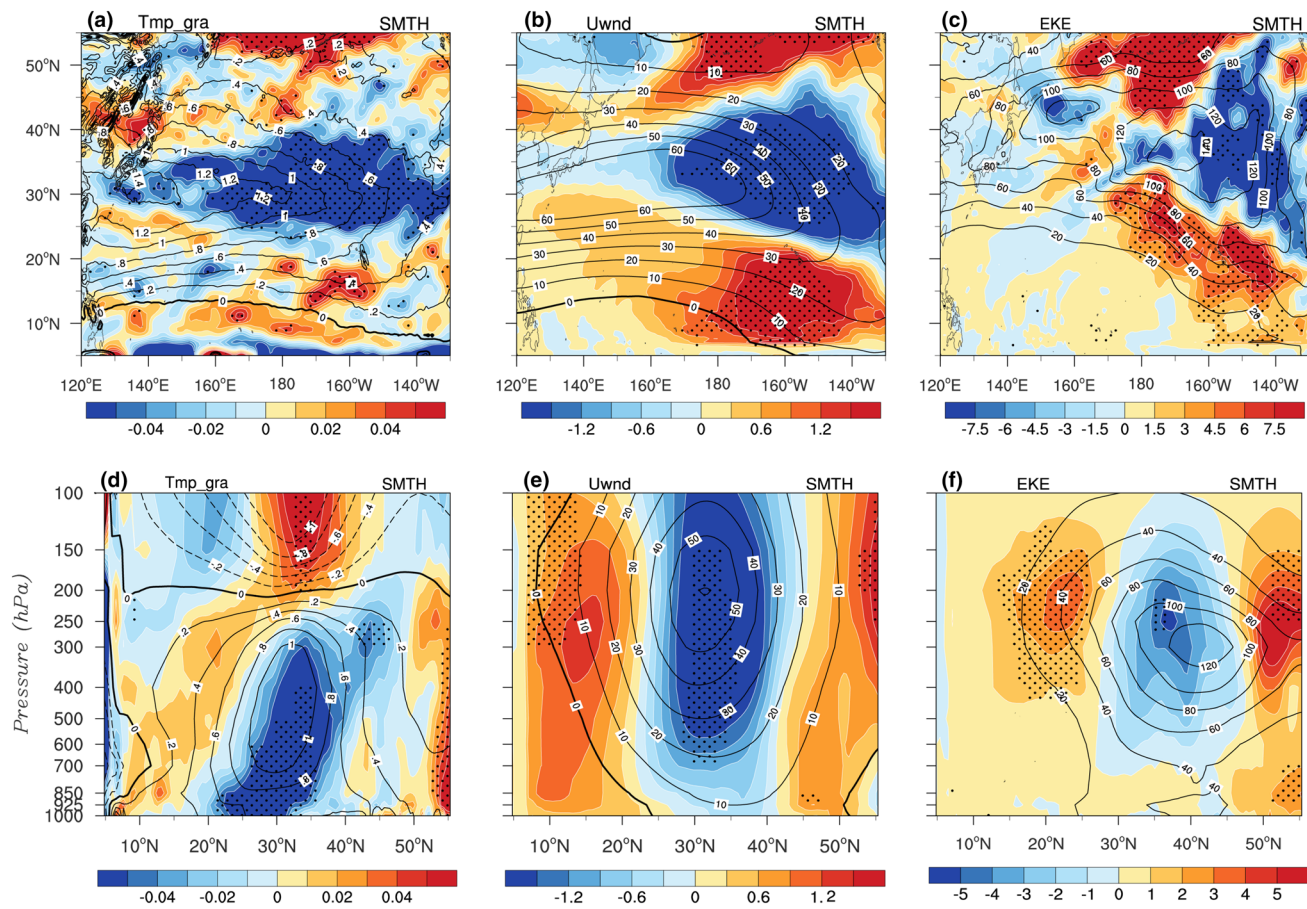


Fig. 14 As in Fig. 10, but for shadings show the atmospheric anomalies between SMTH-STFZ and CNTL experiments

Acknowledgements All the authors share the first author. This work has benefited from discussions with Prof. William Perrie of BIO. The authors thank the anonymous reviewers for their valuable comments and suggestions, and Dr. Astrid at University of Bergen for helpful revision. Thanks to the support of the Jiangsu provincial Innovation Center for climate change. This work was supported by the National Key Program for Developing Basic Science (Grant Nos. 2016YFA0600303), the National Natural Science Foundation of China (Grant Nos. 41330420 & 41621005 & 41675064 & 41675067 & 41875086), the Jiangsu Province Science Foundation (Grant No. SBK2015020577). This work was jointly supported by the Jiangsu Collaborative Innovation Center of Climate Change and Key Laboratory Project Foundation (Grant No. KLME1501). The NCEP/FNL reanalysis data used in this study was obtained from <http://rda.ucar.edu/datasets/ds083.2>, the HadISST data was from <http://www.metoffice.gov.uk/hadobs/hadisst/>, and the OISST data was from <https://www.esrl.noaa.gov/psd/data/gridded/data.noaa.oisst.v2.highres.html>.

Open Access This article is distributed under the terms of the Creative Commons Attribution 4.0 International License (<http://creativecommons.org/licenses/by/4.0/>), which permits unrestricted use, distribution, and reproduction in any medium, provided you give appropriate credit to the original author(s) and the source, provide a link to the Creative Commons license, and indicate if changes were made.

References

- Fang J, Yang XQ (2016) Structure and dynamics of decadal anomalies in the wintertime midlatitude North Pacific ocean–atmosphere system. *Clim Dyn* 47(5–6):1–19
- Frankignoul C, Sennéchal N, Kwon Y, Alexander M (2011) Influence of the meridional shifts of the Kuroshio and the Oyashio Extensions on the atmospheric circulation. *J Clim* 24:762–777. <https://doi.org/10.1175/2010JCLI3731.1>
- Gan B, Wu L (2013) Seasonal and long-term coupling between winter-time storm tracks and surface temperature in the North Pacific. *J Clim* 26:6123–6136. <https://doi.org/10.1175/JCLI-D-12-00724.1>
- Hoskins BJ, Valdes PJ (1990) On the existence of storm-tracks. *J Atmos Sci* 47(15):1854–1864
- Kobashi F, Xie SP, Iwasaka N, Sakamoto T (2008) Deep atmospheric response to the North Pacific oceanic subtropical front in spring. *J Clim* 21(22):5960–5975
- Kosaka Y, Nakamura H (2008) A comparative study on the dynamics of the Pacific–Japan (PJ) teleconnection pattern based on reanalysis datasets, *Sci. Online Lett Atmos* 4:9–12
- Kuwano-Yoshida A, Minobe S (2017) Storm track response to SST fronts in the Northwestern Pacific region in an AGCM. *J Clim* 30:1081–1102. <https://doi.org/10.1175/JCLI-D-16-0331>
- Lau NC, Holopainen E (1984) Transient eddy forcing of the time-mean flow as identified by geopotential tendencies. *J Atmos Sci* 41:313–328

- Mshadek R, Frankignoul C, Li LZX (2001) Mechanisms of the atmospheric response to North Atlantic multidecadal variability: a model study. *Clim Dyn* 36:1255–1276
- Nakamura M, Yamane S (2010) Dominant anomaly patterns in the near-surface baroclinicity and accompanying anomalies in the atmosphere and oceans. Part II: North Pacific basin. *J Clim* 23(24):6445–6467
- Nakamura H, Lin G, Yamagata T (1997) Decadal climate variability in the North Pacific during the recent decades. *Bull Am Meteorol Soc* 78(10):2215–2225
- Nakamura H, Sampe T, Goto A, Ohfuchi W, Xie SP (2008) On the importance of midlatitude oceanic frontal zones for the mean state and dominant variability in the tropospheric circulation. *Geophys Res Lett* 35:L15709. <https://doi.org/10.1029/2008GL034010>
- O'Reilly CH, Czaja A (2015) The response of the Pacific storm track and atmospheric circulation to Kuroshio Extension variability. *Quart J R Meteorol Soc*. <https://doi.org/10.1002/qj.2334> (in press)
- Parfitt R,A, Czaja S, Minobe, Kuwano-Yoshida A (2016) The atmospheric frontal response to SST perturbations in the Gulf Stream region. *Geophys Res Lett* 43(5):2299–2306
- Peng S, Robinson WA, Hoerling MP (1997) The modeled atmospheric response to midlatitude SST anomalies and its dependence on background circulation states. *J Clim* 10:971–987
- Rayner NA, Parker DE, Horton EB, Folland CK, Alexander LV, Rowell DP (2002) Global analyses of SST sea ice and night marine air temperature since the late nineteenth century. *J Geophys Res* 108:4407
- Reynolds RW, Smith TM, Liu C, Chelton DB, Casey KS, Schlax MG (2007) Daily high-resolution-blended analyses for sea surface temperature. *J Clim* 20(22):5473–5496
- Small RJ, Tomas RA, Bryan FO (2014) Storm track response to ocean fronts in a global high-resolution climate model. *Clim Dyn* 43(3–4):805–828
- Taguchi B, Nakamura H, Nonaka M, Komori N, Kuwano-Yoshida A, Takaya K, Goto A (2012) Seasonal evolutions of atmospheric response to decadal SST anomalies in the North Pacific subarctic frontal zone: observations and a coupled model simulation. *J Clim* 25:111–139. <https://doi.org/10.1175/JCLI-D-11-00046.1>
- Wang LY, Hu HB, Yang XQ, Ren XJ (2016) Atmospheric eddy anomalies associated with the wintertime North Pacific subtropical front strength and their influences on the seasonal-mean atmosphere. *Sci China Earth Sci* 59:1–15. <https://doi.org/10.1007/s11430-016-5331-7>
- Wang LY, Yang XQ, Yang DJ, Xie Q, Fang JB, Sun XG (2017) Two typical modes in the variabilities of wintertime North Pacific basin-scale oceanic fronts and associated atmospheric eddy-driven jet. *Atmos Sci Lett*. <https://doi.org/10.1002/asl.766>
- Wills SM, Thompson DWJ, Ciasto LM (2016) On the observed relationships between variability in gulf stream sea surface temperatures and the atmospheric circulation over the North Atlantic. *J Clim* 29(10):3719–3730
- Yao Y, Zhong Z, Yang XQ (2016) Numerical experiments of the storm track sensitivity to oceanic frontal strength within the Kuroshio/Oyashio Extensions. *J Geophys Res: Atmos* 121(6):2888–2900
- Zhang LY, Xu HM, Shi N, Deng JC (2017) Responses of the East Asian jet stream to the North Pacific subtropical front in spring. *Adv Atmos Sci* 34:144–156